Improving Component Substitution Pansharpening Through Multivariate Regression of MS+Pan Data

Bruno Aiazzi, Stefano Baronti, *Member, IEEE*, and Massimo Selva

***Abstract*—In this paper, multivariate regression is adopted to improve spectral quality, without diminishing spatial quality, in image fusion methods based on the well-established component substitution (CS) approach. A general scheme that is capable of modeling any CS image fusion method is presented and discussed. According to this scheme, a generalized intensity component is defined as the weighted average of the multispectral (MS) bands. The weights are obtained as regression coefficients between the MS bands and the spatially degraded panchromatic (Pan) image, with the aim of capturing the spectral responses of the sensors. Once it has been integrated into the Gram–Schmidt spectral-sharpening method, which is implemented in Environment for Visualizing Images (ENVI) program, and into the generalized intensity-hue-saturation fusion method, the proposed preprocessing module allows the production of fused images of the same spatial sharpness but of increased spectral quality with respect to the standard implementations. In addition, quantitative scores carried out on spatially degraded data clearly confirm the superiority of the enhanced methods over their baselines.**

***Index Terms*—Component substitution (CS) pansharpening, Gram–Schmidt (GS) spectral sharpening, IKONOS satellite data, image fusion, intensity-hue-saturation (IHS) transform, multispectral (MS) imagery, multivariate regression, QuickBird images.**

I. Introduction

REMOTE sensing image fusion techniques aim at integrating the information conveyed by the data acquired with different spatial and spectral resolutions from satellite or aerial platforms in order to obtain images of higher quality. Generally, a gold reference is not available to evaluate the efficacy of a fusion method. Thus, quality evaluation should refer to the aims of the fusion process [1]. The most straightforward goal is photo-analysis, but also such automated tasks as features extraction and segmentation/classification have been found to benefit from the fusion [2]–[4]. A variety of image fusion techniques is devoted to merge multispectral (MS) and panchromatic (Pan) images, which exhibit complementary characteristics of spatial and spectral resolutions [5], [6]. Among these techniques, component substitution (CS) methods [7] are attractive because they are fast and easy to implement and they allow user's expectations to be fulfilled most of the time.

A forerunner for CS techniques is the intensity-hue-saturation (IHS) method [8]. This algorithm is suitable when exactly three MS bands are concerned since the IHS transform is defined for three components only. First, the IHS transform is applied to the spectral bands, once they have been registered to the Pan image. Then, the intensity component $\mathbf{I}$ is replaced with the high-resolution Pan $\mathbf{P}$. The fused bands are finally obtained via an inverse IHS. Usually, $\mathbf{P}$ is histogram-matched, i.e., radiometrically transformed by a constant gain and bias in such a way that it exhibits mean and variance that are the same as $\mathbf{I}$, before substitution is carried out. However, since the histogram-matched Pan and the intensity component do not generally have the same radiometry, i.e., local mean, when the fusion result is displayed in color composition, large spectral distortions may be noticed as color changes. This effect occurs because the spectral response of $\mathbf{I}$, as synthesized by means of the MS bands, may be far different from that of Pan. Thus, also slowly space-varying radiance offsets, and not only spatial details, are locally injected.

When more than three bands are available, a viable solution is used to define a generalized IHS (GIHS) transform by including the response of the near-infrared (NIR) band into the intensity component [9]. In this case, $\mathbf{I}$ is obtained by weighting each band with a set of coefficients. The choice of these weights can be related to the spectral responses of the Pan and MS bands by considering the spectral characteristics of the sensors, as in [9] and [10], where prefixed values are adopted.

An alternative to the IHS techniques is principal component analysis (PCA). Being analogous to the IHS scheme, the Pan image is substituted to the first principal component (PC1). Histogram matching of Pan to PC1 is mandatory before substitution because the mean and variance of PC1 are generally far greater than those of Pan. It is well established that PCA performances are better than those of IHS [5] and, in particular, that the spectral distortion in the fused bands is usually less noticeable, even if it cannot completely be avoided. Generally speaking, if the spectral responses of the MS bands are not perfectly overlapped with the bandwidth of Pan, as it happens with the most advanced very high resolution imagers, namely, IKONOS and QuickBird, IHS- and PCA-based methods may yield poor results in terms of spectral fidelity [11].

Another CS technique reported in the literature is Gram–Schmidt (GS) spectral sharpening, which was invented by Laben and Brower in 1998 and patented by Eastman Kodak [12]. The GS method is widely used since it has been implemented in the Environment for Visualizing Images (ENVI) program package. It has two operational modes, depending on how the low-resolution version of the Pan image that is used in the forward GS transformation is defined. In the first case, which will be referred to as "mode 1" or GS1, the low-pass

Manuscript received October 18, 2006; revised March 30, 2007.

The authors are with the Institute of Applied Physics "Nello Carrara" CNR Area di Ricerca di Firenze (IFAC-CNR), 50019 Florence, Italy (e-mail: b.aiazzi@ifac.cnr.it; s.baronti@ifac.cnr.it; m.selva@ifac.cnr.it).

Color versions of one or more of the figures in this paper are available online at http://ieeexplore.ieee.org.

Digital Object Identifier 10.1109/TGRS.2007.901007

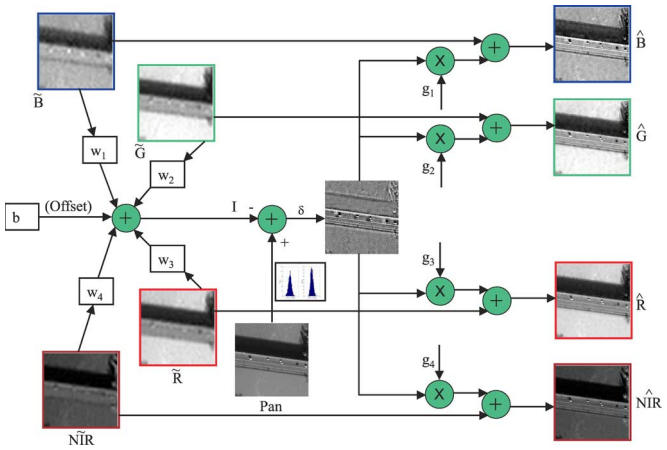

Fig. 1. General scheme of fusion methods based on CS. The aim of weights w_i is to synthesize an intensity image ($\mathbf{I}$) similar to the original Pan image. The weights g_i determine the amounts of detail that are added to the expanded MS bands.

approximation is computed by the ENVI program as the average of the MS bands, which are given as input to the procedure. In the other case, which will be referred to as "mode 2" or GS2, the approximation is preliminarily provided by the user by means of a low-pass filtering and a decimation of the Pan image which is entered into the procedure with the MS bands.

Although the spectral quality of CS fusion results may be sufficient for most applications and users, methods based on injecting zero-mean high-pass spatial details, which are taken from the Pan image without resorting to any transformation, have been extensively studied to definitely overcome the inconvenience of spectral distortion. Multiresolution analysis (MRA) provides effective tools, like wavelets and Laplacian pyramids [13]–[17], to help carry out the data fusion tasks. However, in the case of high-pass detail injection, spatial distortions may occur in fusion products, which are typically caused by ringing or aliasing effects, originating shifts, or blur of contours and textures. These drawbacks, which may be as annoying as spectral distortions, are emphasized by a misregistration between MS and Pan data, especially if the MRA underlying detail injection is not shift-invariant [15], [18].

Due to their impressive spatial quality and to their low computational cost, CS techniques are still investigated by the research community, with the objective of upgrading their spectral accuracy. In this perspective, the contribution of this paper is to define and discuss a general scheme that is capable of modeling any CS-based method, and thus, it is suitable to improve its performances. In particular, two CS fusion methods, namely, the fast GIHS with spectral adjustment [9] and the GS spectral sharpening of ENVI, are considered. The general scheme reported in Fig. 1 defines a generalized intensity component as the weighted average of the MS bands. By applying an optimization method such as a standard linear regression algorithm in calculating the weights, an evident improvement with respect to the performances of standard GIHS and GS methods is obtained. The computed coefficients are satisfactorily capable of matching the spectral responses of MS and Pan.

This paper is organized as follows. GS spectral sharpening is briefly reviewed in Section II. The general scheme of the CS methods is reported in Section III, while the proposed enhancement is motivated and described in Section IV for both the GS and GIHS fusion schemes. Quantitative and qualitative results are reported and discussed in Section V. Eventually, the conclusion is drawn in Section VI.

II. GS Spectral Sharpening

In the GS method, as described by its inventors [12], the spatial resolution of the MS image is enhanced by merging the high-resolution Pan image with the low spatial resolution MS bands. According to the authors' description, the main steps of this method are the following.

1) A lower spatial resolution Pan image is simulated at the same scale of Pan.
2) The GS transformation is performed on the simulated lower spatial resolution Pan image together with the plurality of lower spatial resolution spectral band images resampled at the same scale of Pan. The simulated lower spatial resolution Pan image is employed as the first band in the GS transformation.
3) The statistics of the higher spatial resolution Pan image is adjusted to match the statistics of the first transform band that results from the GS transformation to produce a modified higher spatial resolution Pan image.
4) The modified higher spatial resolution Pan image is substituted for the first transform band that results from the GS transformation to produce a new set of transform bands.
5) The inverse GS transformation is performed on the new set of transform bands to produce the enhanced spatial-resolution MS image.

The presence of some freedom in step 1) determines the two options of the ENVI package that have been described in Section I as GS1 and GS2.

In GS1, the ENVI procedure is responsible in computing the simulated low-resolution Pan image that is obtained as the pixel average of the MS bands. In GS2, it is the user's task to produce the synthetic Pan image that is usually obtained by preliminarily low-pass filtering and, then, decimating the Pan image. The major difference in the results between these two modalities, which is mostly noticeable in true-color display, is that GS1 exhibits an outstanding spatial quality, but spectral distortions with respect the resampled MS image may occur because the average of the MS spectral bands is not likely to have the same radiometry as the Pan image. Instead, GS2 is unaffected by spectral distortion but generally suffers from a lower sharpness and spatial enhancement, which is possibly due to improper digital filtering of the Pan image [17] or subpixel misregistration. This effect is noticeable for small objects appearing on a quasi-constant background.

III. General CS Scheme

Let us consider the fusion scheme in Fig. 1. The original MS bands $\mathbf{B}$, $\mathbf{G}$, $\mathbf{R}$, and $\mathbf{NIR}$ are preliminarily expanded to the same spatial scale of the full-resolution Pan image $\mathbf{P}$ to obtain a new data set $\tilde{\mathbf{B}}$, $\tilde{\mathbf{G}}$, $\tilde{\mathbf{R}}$, and $\mathbf{N\tilde{I}R}$. The expanded MS bands

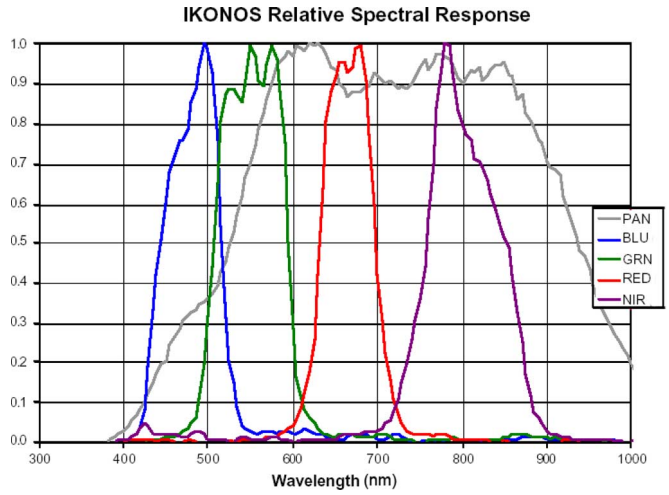

Fig. 2. IKONOS spectral responses.

are weighted by the coefficients $\{w_i\}$ to generate a synthetic intensity component $\mathbf{I}$

$$\mathbf{I} = w_1 \cdot \tilde{\mathbf{B}} + w_2 \cdot \tilde{\mathbf{G}} + w_3 \cdot \tilde{\mathbf{R}} + w_4 \cdot \tilde{\mathbf{NIR}} + \boldsymbol{b}. \quad (1)$$

The constant parameter $\boldsymbol{b}$ is an offset image introduced in the model to consider the additive component that may arise from the acquisition process and from the sensor spectral responses reported in Fig. 2 for IKONOS imager. In fact, the Pan sensor collects photons in a spectral band that is larger than that of the MS channels, and spectral gaps exist between MS spectral responses. Taking into account the offset brings a stabilization of the weights $\{w_i\}$ at different spatial scales.

Afterward, $\mathbf{I}$ is subtracted from $\mathbf{P}$ to produce a detail image $\boldsymbol{\delta}$, i.e.,

$$\boldsymbol{\delta} = \mathbf{P} - \mathbf{I}. \quad (2)$$

A second set of coefficients $\{g_i\}$ is adopted to modulate the detail image $\boldsymbol{\delta}$ before its addition to the expanded data set in order to yield the final fused bands, i.e., $\hat{\mathbf{B}}$, $\hat{\mathbf{G}}$, $\hat{\mathbf{R}}$, and $\hat{\mathbf{NIR}}$.

A histogram matching is usually performed on $\mathbf{P}$ to match its mean and standard deviation to those of the synthesized $\mathbf{I}$ component. This procedure has the objective of reducing spectral distortions that are caused by the spectral mismatch between $\mathbf{I}$ and $\mathbf{P}$ images, as discussed in Section II.

The scheme described in Fig. 1 is general and is suitable in describing any CS-based fusion algorithm, depending on the values of the two sets of weights $\{w_i\}$ and $\{g_i\}$. This is evidenced in the following discussion, where $\boldsymbol{b}$ is assumed to be equal to zero, without losing generality.

The expressions of the weights w_i and g_i for the considered CS-based methods are summarized in Table I.

Actually, the IHS procedure is equivalent to the injection, i.e., addition, of the difference between $\mathbf{P}$ and $\mathbf{I}$ into the resampled MS bands [19]. Consequently, IHS fusion method can easily be described by the scheme when the weights are taken as $w_1 = w_2 = w_3 = 1/3$, $g_1 = g_2 = g_3 = 1$, and $w_4 = g_4 = 0$.

As previously stated, the IHS method can be generalized. Hereinafter, GIHS will denote a case in which $\mathbf{I}$ is simply the average of four MS bands, while for the GIHS with fixed weights, which is introduced in [9] (GIHSF), $\mathbf{I}$ is the weighted average of the four MS bands.

TABLE I
EXPRESSIONS FOR THE WEIGHTS OF THE SCHEME REPORTED IN FIG. 1 RELATIVE TO THE VARIOUS CS-BASED METHODS

Method	w_1	w_2	w_3	w_4	$\mathbf{b}$	g_1	g_2	g_3	g_4
IHS	1/3	1/3	1/3	0	0	1	1	1	0
GIHS	1/4	1/4	1/4	1/4	0	1	1	1	1
GIHSF	1/12	1/4	1/3	1/3	0	1	1	1	1
GIHSA	$\hat{w}_1$	$\hat{w}_2$	$\hat{w}_3$	$\hat{w}_4$	$\hat{\boldsymbol{b}}$	1	1	1	1
PCA	x_{11}	x_{12}	x_{13}	x_{14}	0	x_{11}	x_{12}	x_{13}	x_{14}
GS1	1/4	1/4	1/4	1/4	0	$\frac{cov(\mathbf{I},\tilde{\mathbf{B}})}{var(\mathbf{I})}$	$\frac{cov(\mathbf{I},\tilde{\mathbf{G}})}{var(\mathbf{I})}$	$\frac{cov(\mathbf{I},\tilde{\mathbf{R}})}{var(\mathbf{I})}$	$\frac{cov(\mathbf{I},\tilde{\mathbf{NIR}})}{var(\mathbf{I})}$
GS2	nd	nd	nd	nd	nd	$\frac{cov(\mathbf{I},\tilde{\mathbf{B}})}{var(\mathbf{I})}$	$\frac{cov(\mathbf{I},\tilde{\mathbf{G}})}{var(\mathbf{I})}$	$\frac{cov(\mathbf{I},\tilde{\mathbf{R}})}{var(\mathbf{I})}$	$\frac{cov(\mathbf{I},\tilde{\mathbf{NIR}})}{var(\mathbf{I})}$
GSF	1/12	1/4	1/3	1/3	0	$\frac{cov(\mathbf{I},\tilde{\mathbf{B}})}{var(\mathbf{I})}$	$\frac{cov(\mathbf{I},\tilde{\mathbf{G}})}{var(\mathbf{I})}$	$\frac{cov(\mathbf{I},\tilde{\mathbf{R}})}{var(\mathbf{I})}$	$\frac{cov(\mathbf{I},\tilde{\mathbf{NIR}})}{var(\mathbf{I})}$
GSA	$\hat{w}_1$	$\hat{w}_2$	$\hat{w}_3$	$\hat{w}_4$	$\hat{\boldsymbol{b}}$	$\frac{cov(\mathbf{I},\tilde{\mathbf{B}})}{var(\mathbf{I})}$	$\frac{cov(\mathbf{I},\tilde{\mathbf{G}})}{var(\mathbf{I})}$	$\frac{cov(\mathbf{I},\tilde{\mathbf{R}})}{var(\mathbf{I})}$	$\frac{cov(\mathbf{I},\tilde{\mathbf{NIR}})}{var(\mathbf{I})}$

With regard to GIHS, an exhaustive mathematical formulation is reported in [9]. Its description and implementation is immediate from the scheme of Fig. 1.

Being analogous to GIHS, for GS1, $\mathbf{I}$ is the average of the four MS bands. A variant of this scheme that is considered in this paper (GSF hereinafter) is obtained by synthesizing $\mathbf{I}$ with the set of $\{w_i\}$ reported in [9], which is the same as GIHSF.

GS2 is obtained in the scheme of Fig. 1 when a low-pass-filtered version of $\mathbf{P}$ is given instead of $\mathbf{I}$. It is to be noted that GS2 is not strictly a CS method since only $\mathbf{P}$ is utilized in producing spatial details, analogously to the MRA-based methods. Thus, $\{w_i\}$ is not defined in this mode.

In any case, for all the GS-based methods, the ith coefficient g_i is proportional to the covariance value between the synthesized intensity and the expanded ith MS band. The demonstration of this relation is reported in the Appendix.

With regard to PCA, it can easily be shown that, if Pan is histogram-matched to PC1, $w_i = g_i$, with both being the ith component of the first eigenvector $\mathbf{x_1}$ that constitutes the unitary transformation matrix.

The two variants that are proposed in this paper and are described in Section IV, namely, GS adaptive (GSA) and GIHS adaptive (GIHSA), are also reported in Table I.

IV. ENHANCED GS AND GIHS IMAGE FUSION

To understand the influence of spectral response on the fusion procedure for high spatial resolution sensors, as IKONOS and QuickBird, the relative spectral response plots of the IKONOS spectral channels, which are reported in Fig. 2, have been considered. Ideally, the MS bands (B, G, R, and NIR) should be disjoint and should entirely fall within the bandwidth of Pan. From Fig. 2, however, it appears that the G and B bands are largely overlapped and that the B band mostly falls outside the 3-dB cutoff of the Pan spectral band. Furthermore, the spectral response of Pan is extended beyond the NIR band. The color distortion problem in fusion stems from such mismatches and, in particular, from the fact that the synthetic intensity of the methods with equal weights (IHS, GIHS, and GS1) does not reflect the spectral response of Fig. 2 since it is obtained as a plain average of MS bands. For example, vegetation appears of relatively high reflectance in the NIR band and Pan image, while its reflectance is low in the visible (R, G, and B) bands.

As a consequence, the radiometric values of vegetation areas is likely to be much smaller in the synthetic intensity than in the true Pan. This effect causes the injection in the fused MS bands of a radiance offset, which may give rise to color distortion.

In order to avoid this drawback, the idea reported in [20] and [21] is to generate the synthetic intensity in such a way that the spectral response of the sensor is considered, by differently weighting the contributions coming from the MS spectral channels.

These methods, however, only consider the nominal spectral responses when available. Actually, the influence of other phenomena, such as on-orbit working conditions, variability of the observed scene, and postprocessing effects, can significantly modify the nominal spectral response. In particular, atmospheric influence depends on the viewing angle since the scattering effect is related to the wavelength and on atmospheric conditions.

A viable solution is to perform a linear regression between Pan and MS bands. Thus, in the proposed scheme, a synthetic intensity, having a minimum mean-square error (mse) with respect to the reduced Pan, is computed. The steps of the procedure are the following.

1) Reduce the original full-resolution Pan image to the spatial scale of the MS image by means of low-pass filtering and decimation. Let us denote this image as $\breve{\mathbf{P}}$.
2) Assume that

$$\breve{\mathbf{I}} = w_1 \cdot \mathbf{B} + w_2 \cdot \mathbf{G} + w_3 \cdot \mathbf{R} + w_4 \cdot \mathbf{NIR} + \boldsymbol{b} \quad (3)$$

and estimate the set of coefficients $\hat{w}_1$, $\hat{w}_2$, $\hat{w}_3$, $\hat{w}_4$, and $\hat{b}$ by means of a linear regression algorithm [22] in order to minimize the mse between $\breve{\mathbf{P}}$ and $\breve{\mathbf{I}}$.
3) Calculate intensity $\mathbf{I}$ at the scale of $\mathbf{P}$ by utilizing the set of coefficients determined at step 2)

$$\mathbf{I} = \hat{w}_1 \cdot \tilde{\mathbf{B}} + \hat{w}_2 \cdot \tilde{\mathbf{G}} + \hat{w}_3 \cdot \tilde{\mathbf{R}} + \hat{w}_4 \cdot \tilde{\mathbf{NIR}} + \hat{\boldsymbol{b}}. \quad (4)$$

The implicit assumption that is done in step 3) is that the regression coefficients that are computed at the scale of the MS image are practically the same as those that would be computed at the scale of the original Pan image, if MS observations were available at full spatial resolution. This is to assume that the spectral responses of the data set are practically unaffected by the change of the spatial resolution.

In this paper, the estimation of $\mathbf{I}$ using (4) is applied to GIHS, and it is where the algorithm denoted as GIHSA originates.

With regard to GS, since the ENVI procedure in "mode 2" accepts a synthetic intensity as input at the resolution of the MS image, the intensity $\breve{\mathbf{I}}$ that is estimated by (3) is provided to the ENVI module for the implementation of the proposed regression strategy. This method is hereinafter referred to as GSA.

In Section V, the proposed GSA and GIHSA methods are assessed through comparisons with the other algorithms on two different high spatial resolution data sets acquired by IKONOS and QuickBird sensors.

V. Results

Results have been assessed on two data sets acquired by IKONOS and QuickBird satellites. Both qualitative and quantitative assessments have been performed.

Evaluations are not oriented to a specific application task but rather to photo-analysis. However, to give an idea on how the methods perform on different landscapes, quantitative scores are also reported and discussed for three classes of land-use.

Quantitative assessments are obtained by degrading the spatial resolution of all original images by a factor of four and by performing fusion on such images [23]. The comparison of fused original images allows such global synthetic scores as Q4 [24], spectral angle mapper (SAM), and erreur relative globale adimensionnelle de synthése (ERGAS) [14], [16] to be computed.

SAM and ERGAS are distortion figures and should take values as low as possible (ideally zero). ERGAS is mainly related to radiometric distortion, while SAM is related to angular distortion.

Conversely, Q4 represents a quality index and should be as high as possible (ideally one). Q4 takes into account the contrast, mean bias, and similarity between images [24].

It should be noted that, since the regression strategy minimizes the mse between $\mathbf{P}$ and $\mathbf{I}$ images, improvements should be expected, in particular, for ERGAS.

Quantitative scores have been reported on the whole processed images for both IKONOS and QuickBird test images. For the IKONOS test image, in order to verify the behavior of the fusion algorithms on different landscapes, scores have been computed by identifying three different land classes: urban, vegetated, and homogeneous areas.

The next two sections present and discuss the results.

A. IKONOS

Fig. 3 refers to the IKONOS data set and shows a 512×512 detail of the whole 2048×2048 11-bit image of the area of Toulouse, France, that has been processed. The full-resolution Pan image is reported in Fig. 3(a), while the original true-color MS image, which is expanded to the scale of Pan, is reported in Fig. 3(b). Fig. 3(b) is assumed as the reference in evaluating color distortions. Fig. 3(c) shows the result of GS1, i.e., the synthetic low-resolution Pan is obtained as the pixel average of the four MS bands. The spatial enhancement is impressive; however, some color distortion appears on the green areas on the left of the river and on the river itself. The green areas are too bright while the color of the river is too dark.

These spectral distortions are not present in Fig. 3(d), which shows the outcome of GS2, i.e., the synthetic Pan is obtained as a low-pass-filtered version of the full-resolution Pan. As a counterpart, Fig. 3(d) is less sharp than Fig. 3(c). Fig. 3(e) and (f) results from the proposed modified versions. Fig. 3(e) has been obtained by synthesizing the low-resolution Pan as a weighted sum of all spectral bands (GSF), according to the fixed weights proposed by [9] and reported in Table I. Fig. 3(e) appears as sharp as Fig. 3(c), but the spectral distortion is mitigated. The result obtained with the adaptive

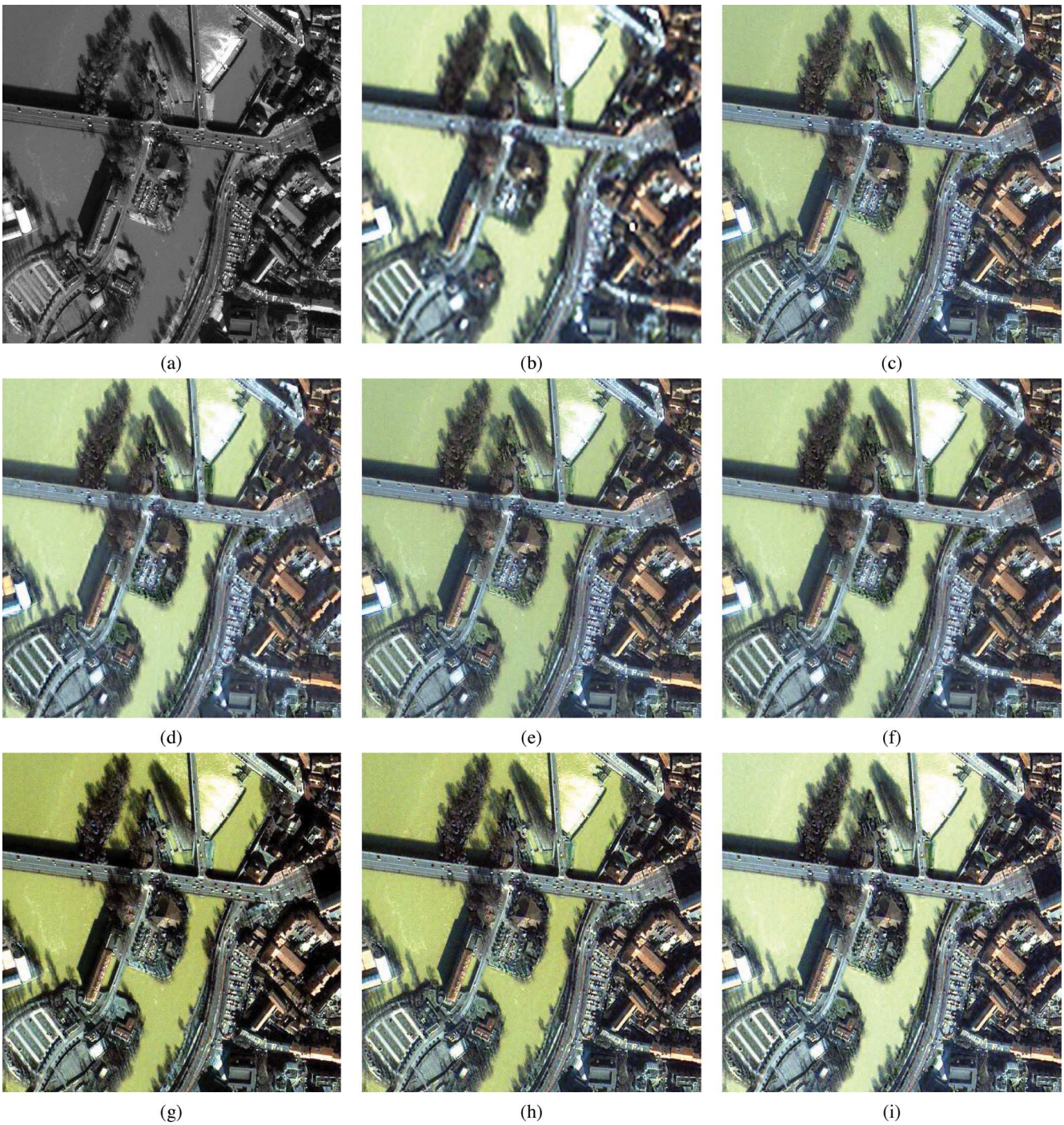

Fig. 3. Examples of a full-scale spatial enhancement of fusion algorithms displayed as 512 × 512 true-color compositions at a 1-m pixel spacing for the IKONOS image. (a) Original Pan image. (b) Original MS bands (4 m) resampled to the scale of Pan image (1 m). (c) GS "mode 1" fusion (GS1). (d) GS "mode 2" (GS2). (e) GS with fixed weights (GSF). (f) GS with adaptive weights (GSA). (g) GIHS with equal weights (GIHS). (h) GIHS with unequal fixed weights (GIHSF). (i) GIHS with adaptive weights (GIHSA).

preprocessing (GSA) is shown in Fig. 3(f). The weights calculated on the whole image are reported in Table II. The spectral fidelity with respect to the original MS data of Fig. 3(b) is impressive, while spatial details appear as sharp as those in Fig. 3(c).

Fig. 3(g) reports the result obtained by applying GIHS, while Fig. 3(h) refers to GIHSF. Both methods have been implemented in the same way as described in [9]. Spatial details are very sharp, but spectral distortions are evident in both images. Fig. 3(i) shows the result obtained by the proposed GIHSA. Spectral fidelity is very high and comparable to that of GS2 and the proposed GSA.

TABLE II
REGRESSION WEIGHTS COMPUTED BETWEEN THE ORIGINAL 4-m MS BANDS AND THE REDUCED 4-m PAN FOR IKONOS IMAGE

Satellite	$\hat{w}_1$	$\hat{w}_2$	$\hat{w}_3$	$\hat{w}_4$	$\hat{b}$
IKONOS	0.067	0.189	0.228	0.319	25.028

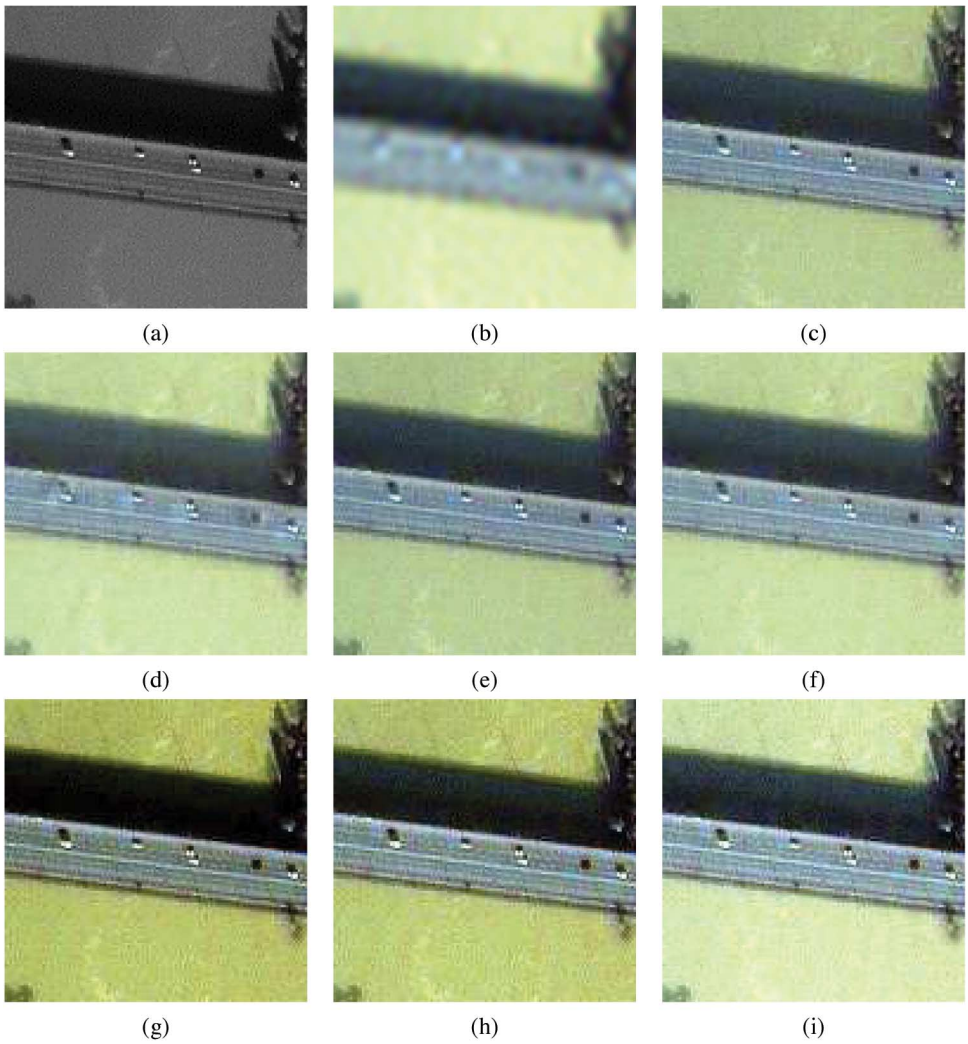

Fig. 4. IKONOS. Results of fusion algorithms displayed as 128 × 128 true-color compositions at a 1-m pixel spacing. (a) Original Pan image. (b) Original MS bands (4 m) resampled to the scale of Pan image (1 m). (c) GS1. (d) GS2. (e) GSF. (f) GSA. (g) GIHS. (h) GIHSF. (i) GIHSA.

Small 128 × 128 details produced by all the methods, which are extracted from the image shown in Fig. 3, are displayed in Fig. 4; the disposition of the images is the same as in Fig. 3. Spectral distortions are noticeable as changes in color hue of the river with respect to the resampled low-resolution original MS of Fig. 4(b). The images of Fig. 4(f) and (i), which are for GSA and GIHSA, respectively, exhibit high spectral and spatial quality. All fused images show impressive spatial details since all are derived from CS methods. Spatial distortions are only noticeable in Fig. 4(d) (GS2), especially for the cars on the bridge. However, GS2 *de facto* belongs to the MRA methods because the synthetic intensity component is obtained by low-pass filtering and decimating the original Pan image.

Visual judgement is corroborated by quantitative assessments. Score values are reported in Table III for the whole 2048 × 2048 image and show that the proposed regression-based enhancement strategy improves both GS and GIHS fusion algorithms with respect to all other nonadaptive implementations. In particular, GSA results better than GIHSA when considering Q4 and SAM, while GIHSA is superior to GSA regarding ERGAS. Since GIHSA and GSA utilize the same $\mathbf{I}$ component, this is evidently due to the $\{g_i\}$ weights that are different according to Table I. For the IKONOS test image, GIHSA weights are more efficient than those of GSA.

TABLE III
IKONOS: AVERAGE CUMULATIVE QUALITY INDEXES BETWEEN THE ORIGINAL 4-m MS AND THE FUSED IMAGES OBTAINED FROM 16-m MS AND 4-m PAN

4:1	EXP	GS1	GS2	GSF	GSA	GIHS	GIHSF	GIHSA
Q4	.630	.857	.849	.860	.864	.746	.834	.850
SAM (°)	4.85	4.19	4.03	4.06	3.82	4.17	3.92	3.94
ERGAS	5.94	3.83	3.81	3.71	3.55	4.19	3.38	3.23

The only slight exception in Table III is represented by SAM of GIHSF and GIHSA. This is however compensated by the significant improvement of ERGAS. Actually, the mse minimization, in this case, has produced regression coefficients that are not the best for SAM. It was verified during the test phase that a not negligible improvement of SAM of GIHSA is obtained by just slightly decreasing $\hat{w}_1$ and correspondingly

TABLE IV
IKONOS: AVERAGE CUMULATIVE QUALITY INDEXES BETWEEN THE ORIGINAL 4-m MS AND THE FUSED IMAGES ON URBAN AREAS

4:1	EXP	GS1	GS2	GSF	GSA	GIHS	GIHSF	GIHSA
Q4	.617	.866	.873	.866	.870	.830	.811	.839
SAM (°)	5.59	4.51	4.55	4.51	4.43	5.15	5.12	5.17
ERGAS	5.46	3.26	3.20	3.26	3.18	3.56	3.60	3.44

TABLE V
IKONOS: AVERAGE CUMULATIVE QUALITY INDEXES BETWEEN THE ORIGINAL 4-m MS AND THE FUSED IMAGES ON VEGETATED AREAS

4:1	EXP	GS1	GS2	GSF	GSA	GIHS	GIHSF	GIHSA
Q4	.645	.793	.817	.793	.844	.785	.760	.805
SAM (°)	3.22	3.04	3.08	3.04	2.72	3.08	3.07	3.07
ERGAS	3.14	2.31	2.27	2.31	2.00	2.14	2.16	2.03

TABLE VI
IKONOS: AVERAGE CUMULATIVE QUALITY INDEXES BETWEEN THE ORIGINAL 4-m MS AND THE FUSED IMAGES ON HOMOGENEOUS AREAS

4:1	EXP	GS1	GS2	GSF	GSA	GIHS	GIHSF	GIHSA
Q4	.876	.689	.869	.687	.860	.662	.665	.910
SAM (°)	1.03	3.64	1.24	3.64	1.26	2.03	1.81	1.01
ERGAS	1.23	5.15	1.15	5.15	1.17	3.73	3.16	0.90

increasing $\hat{w}_2$. As expected, the improvement of SAM is paid in terms of ERGAS.

Tables IV–VI report the quality indices that have been evaluated on the three classes of urban, vegetated, and homogeneous areas, respectively. The values of these indices depend on the quantity of details that is present on the landscape, as one might expect. Urban class figures are the worst, while those of the homogeneous class are the best. GSA and GIHSA are always better than their nonadaptive counterparts, with only few minor exceptions; also in the other cases, their score is quite near to the best one. In any case, their ERGAS is always the lowest. Another general consideration is that the fixed weights that are defined in [9] do not perform better than the baseline in which all the weights are equal. This is a firm indication that fixed coefficients are not suitable in coping with such variabilities as those introduced by scene variations, atmospheric conditions, and attitude or aging of the acquisition platform. Conversely, regression strategy guarantees a greater flexibility and more steady performances. The superiority of GSA and GIHSA is evident on the vegetated areas, on which they largely outperform the other schemes, demonstrating that modeling of spectral response is effective on vegetation. The performance of constant weight methods on homogeneous areas (mainly extracted from the river appearing in Fig. 3) is disappointing. Since homogeneous areas are dealt with, the only explanation is that they are not able to efficiently model the local average value of the synthetic intensity image. The ERGAS values are particularly low for GSA, GS2, and GIHSA, demonstrating their effectiveness.

B. QuickBird

In order to assess the fusion algorithms for a different sensor, also a QuickBird data set has been considered. Conversely, from IKONOS, for which spectral responses that are reported in Fig. 2 are accessible, spectral responses of QuickBird have not been made available to our knowledge. This does not represent a problem for GSA and GIHSA since these algorithms estimate their weights from the data. With regard to GSF and GIHSF, performances are computed with the fixed weights reported in [9], which have been found suitable for IKONOS and considered reasonable for QuickBird.

Fig. 5 reports the results of the algorithms on a 128 × 128 detail extracted from the selected 2048 × 2048 11-bit test image. The disposition of the images of Fig. 5 is the same as in Figs. 3 and 4. As a general consideration, differences in the results among methods of the same family are less apparent for QuickBird than for IKONOS. Conversely, differences among GS- and IHS-based methods are more apparent in QuickBird since all IHS methods have the tendency to inject too much blue on the vegetated areas. The correction introduced by the regression algorithm is consistent, but not sufficient to completely avoid this inconvenience. The image produced by GSA and GIHSA appear to be of great quality. GSA colors [Fig. 5(f)] appear consistent with Fig. 5(b), while GIHSA [Fig. 5(i)] appears a little bit bluish, but of great contrast.

The weights calculated from the whole image of GSA and GIHSA are shown in Table VII. If these weights are compared with those of IKONOS that are shown in Table II, the two sets of coefficients have the same trend since they are monotonic in both cases along the wavelength. The B weight $(\hat{w}_1)$ for QuickBird is rather low, but this agrees with the data distribution in the B channel, which is very narrow (low standard deviation). This also explains why images that are produced by the IHS methods are bluish. In fact, images fused by such methods suffer from an over-injection into the blue band.

Table VIII reports the quantitative scores for the selected 2048 × 2048 11-bit images. All the GS-based methods perform better than the IHS-based algorithms. GS2, GSF, and GSA are particularly effective on QuickBird and obtain the best scores. Among the IHS-based algorithms, GIHSF performances are the worst, thus confirming again that the regression strategy of GIHSA is superior to the fixed weight choice.

VI. CONCLUDING REMARKS

Multivariate regression brings advantages in methods based on CS with respect to all the preprocessing methods that have been considered to create the synthetic low-resolution-intensity images. The proposed enhanced strategy is effective in improving the quality of the images fused with GS spectral sharpening and with GIHS and requires only a negligible extra computation with respect to that of the standard implementations. A general model is derived for the CS schemes that allows, in particular, an easy comparison between different fusion strategies. In this framework, regression optimization can be implemented as a preprocessing block, which can easily be introduced in the fusion algorithms to compute the generalized intensity. With regard to GS spectral sharpening, the block can be written in image display language (IDL) and integrated within the ENVI module. Future work will explore different types of optimization strategies that are made possible in the general scheme for CS modeling, with the objective of reducing the gap in performance that presently exists between fusion methods based on CS and the ones based on MRA.

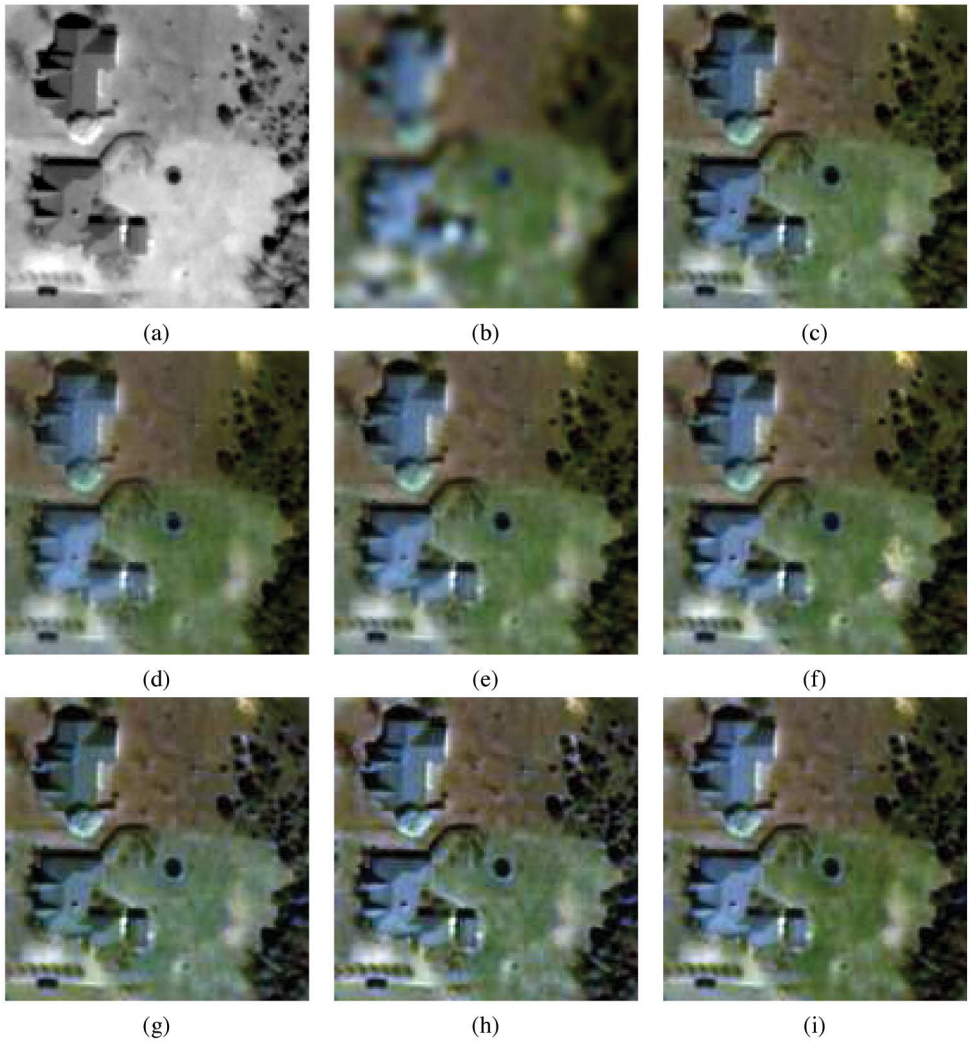

Fig. 5. QuickBird. Results of fusion algorithms displayed as 128 × 128 true-color compositions at a 0.7-m pixel spacing. (a) Original Pan image. (b) Original MS bands (2.8 m) resampled to the scale of Pan image (0.7 m). (c) GS1. (d) GS2. (e) GSF. (f) GSA. (g) GIHS. (h) GIHSF. (i) GIHSA.

TABLE VII
REGRESSION WEIGHTS COMPUTED BETWEEN THE ORIGINAL 2.8-m MS BANDS AND THE REDUCED 2.8-m PAN FOR QUICKBIRD IMAGE

Satellite	$\hat{w}_1$	$\hat{w}_2$	$\hat{w}_3$	$\hat{w}_4$	$\hat{b}$
QuickBird	0.035	0.216	0.387	0.412	4.475

TABLE VIII
QUICKBIRD: AVERAGE CUMULATIVE INDEXES BETWEEN THE ORIGINAL 2.8-m MS AND THE FUSED IMAGES OBTAINED FROM 11.2-m MS AND 2.8-m PAN

4:1	EXP	GS1	GS2	GSF	GSA	GIHS	GIHSF	GIHSA
Q4	.785	.862	.886	.880	.882	.778	.763	.812
SAM (°)	2.50	2.52	2.48	2.48	2.49	3.07	3.14	3.00
ERGAS	2.29	1.96	1.74	1.80	1.76	2.32	2.44	2.09

APPENDIX

Let

$$\mathbf{V} = (\mathbf{I} \quad \tilde{\mathbf{B}} \quad \tilde{\mathbf{G}} \quad \tilde{\mathbf{R}} \quad \mathbf{N\tilde{I}R})$$

be the matrix given as input to the GS transform, where the first column of $\mathbf{V}$ is the simulated intensity $\mathbf{I}$, and $\tilde{\mathbf{B}}$, $\tilde{\mathbf{G}}$, $\tilde{\mathbf{R}}$, and $\mathbf{N\tilde{I}R}$ are the MS bands. All these images are reported at the scale of the high-resolution panchromatic $\mathbf{P}$ and arranged as vectors, which are hereinafter supposed to be zero-mean in order to simplify the notation without losing generality.

Let

$$\mathbf{U} = (\mathbf{GS_1} \quad \mathbf{GS_2} \quad \mathbf{GS_3} \quad \mathbf{GS_4} \quad \mathbf{GS_5})$$

also be the matrix that is obtained as an output of the GS transform applied to $\mathbf{V}$.

The relation between $\mathbf{U}$ and $\mathbf{V}$ is expressed by the forward GS transform

$$\mathbf{U} = \mathbf{V} \cdot \mathbf{C} \tag{5}$$

where $\mathbf{C}$ is a 5 × 5 upper unit triangular matrix, where the nonzero elements, apart from the diagonal ones, are obtained by the GS orthogonalization procedure, as shown in [25]. In this Appendix, the focus is not in evidencing the direct transformation, which is not difficult but formally complicated, but rather in the inverse transform.

From (5), the inverse GS transform is obviously

$$\mathbf{V} = \mathbf{U} \cdot \mathbf{C}^{-1} \tag{6}$$

where the inverse matrix $\mathbf{C^{-1}}$ is again a 5×5 upper unit triangular matrix [25], whose nonzero elements are being easily expressed by

$$C^{-1}(i,j) = c_{ij} = \mathrm{proj}_{\mathbf{u_i}}\mathbf{v_j}, \qquad i \leq j \tag{7}$$

with $\mathrm{proj}_{\mathbf{u_i}}\mathbf{v_j}$ as the orthogonal projection of vector $\mathbf{v_j}$ onto vector $\mathbf{u_i}$, which is given by

$$\mathrm{proj}_{\mathbf{u_i}}\mathbf{v_j} = \frac{\langle \mathbf{u_i}, \mathbf{v_j} \rangle}{\|\mathbf{u_i}\|^2} \tag{8}$$

with $\langle \mathbf{u_i}, \mathbf{v_j} \rangle$ as the scalar product between $\mathbf{u_i}$ and $\mathbf{v_j}$. Since all vectors are zero-mean, the following relation holds:

$$\mathrm{proj}_{\mathbf{u_i}}\mathbf{v_j} = \frac{\mathrm{cov}(\mathbf{u_i}, \mathbf{v_j})}{\mathrm{var}(\mathbf{u_i})}. \tag{9}$$

Note that, from the definition of $\mathbf{C}$ (upper unit triangular matrix), it follows that $\mathbf{GS_1}$ coincides with $\mathbf{I}$.

The GS fusion algorithms substitute $\mathbf{GS_1}$ with the high-resolution panchromatic $\mathbf{P}$ after it has been histogram-matched to $\mathbf{I}$ in the matrix $\mathbf{U}$, thus obtaining a new matrix $\mathbf{U}'$, and then perform the inverse transform. Therefore, the output matrix $\hat{\mathbf{V}}$ is given by

$$\hat{\mathbf{V}} = \mathbf{U}' \cdot \mathbf{C^{-1}}. \tag{10}$$

The fusion products, i.e., the high-resolution MS bands, apart from the average values, are simply obtained starting from the second column in the matrix $\hat{\mathbf{V}}$

$$\hat{\mathbf{V}} = (\mathbf{P} \quad \hat{\mathbf{B}} \quad \hat{\mathbf{G}} \quad \hat{\mathbf{R}} \quad \mathbf{N\hat{I}R}).$$

If $\boldsymbol{\delta}$ denotes the detail image to be injected, we can express $\mathbf{P}$ as

$$\mathbf{P} = \mathbf{P} - \mathbf{I} + \mathbf{I} = \mathbf{I} + \boldsymbol{\delta}. \tag{11}$$

Consequently, the matrix $\mathbf{U}'$ can be written as

$$\mathbf{U}' = \mathbf{U} + (\boldsymbol{\delta} \quad \mathbf{0} \quad \mathbf{0} \quad \mathbf{0} \quad \mathbf{0}) \tag{12}$$

and by applying (6)

$$\hat{\mathbf{V}} = \mathbf{V} + (\boldsymbol{\delta} \quad \mathbf{0} \quad \mathbf{0} \quad \mathbf{0} \quad \mathbf{0}) \cdot \mathbf{C^{-1}}. \tag{13}$$

The final expression for the output matrix $\hat{\mathbf{V}}$ by using (7) is the following:

$$\hat{\mathbf{V}} = \mathbf{V} + (\boldsymbol{\delta} \quad c_{12}\boldsymbol{\delta} \quad c_{13}\boldsymbol{\delta} \quad c_{14}\boldsymbol{\delta} \quad c_{15}\boldsymbol{\delta}) \tag{14}$$

and the coefficient set $\{g_i\}$ for the two GS methods, with reference to the scheme of Fig. 1, is given by

$$g_i = c_{1,i+1}. \tag{15}$$

Eventually, from (9), the set $\{g_i\}$ that is determined by (15) is expressed by the following relations for the $\mathbf{B}$, $\mathbf{G}$, $\mathbf{R}$, and $\mathbf{NIR}$ bands, respectively:

$$\begin{aligned} g_1 &= \frac{\mathrm{cov}(\mathbf{I}, \tilde{\mathbf{B}})}{\mathrm{var}(\mathbf{I})} \\ g_2 &= \frac{\mathrm{cov}(\mathbf{I}, \tilde{\mathbf{G}})}{\mathrm{var}(\mathbf{I})} \\ g_3 &= \frac{\mathrm{cov}(\mathbf{I}, \tilde{\mathbf{R}})}{\mathrm{var}(\mathbf{I})} \\ g_4 &= \frac{\mathrm{cov}(\mathbf{I}, \mathbf{N\tilde{I}R})}{\mathrm{var}(\mathbf{I})}. \end{aligned} \tag{16}$$

ACKNOWLEDGMENT

The authors would like to thank Prof. L. Alparone for his invaluable contribution and stimulating discussions.

REFERENCES

[1] L. Wald, "Some terms of reference in data fusion," *IEEE Trans. Geosci. Remote Sens.*, vol. 37, no. 3, pp. 1190–1193, May 1999.

[2] J. Wahlen, "Comparison of standard and image-filter fusion techniques," in *Data Mining III*, A. Zanasi, C. A. Brebbia, N. F. F. Ebecken, and P. Melli, Eds. Southampton, U.K.: WIT Press, 2002.

[3] Y. Zang and R. Wang, "Multi-resolution and multi-spectral image fusion for urban object extraction," in *Proc. 20th ISPRS Congr.*, 2004, pp. 960–966.

[4] R. Colditz, T. Wehrmann, M. Bachmann, K. Steinnocher, M. Schmidt, G. Strunz, and S. Dech, "Influence of image fusion approaches on classification accuracy: A case study," *Int. J. Remote Sens.*, vol. 27, no. 15, pp. 3311–3335, Aug. 2006.

[5] P. S. Chavez, Jr., S. C. Sides, and J. A. Anderson, "Comparison of three different methods to merge multiresolution and multispectral data: Landsat TM and SPOT panchromatic," *Photogramm. Eng. Remote Sens.*, vol. 57, no. 3, pp. 295–303, 1991.

[6] Z. Wang, D. Ziou, C. Armenakis, D. Li, and Q. Li, "A comparative analysis of image fusion methods," *IEEE Trans. Geosci. Remote Sens.*, vol. 43, no. 6, pp. 1391–1402, Jun. 2005.

[7] V. K. Shettigara, "A generalized component substitution technique for spatial enhancement of multispectral images using a higher resolution data set," *Photogramm. Eng. Remote Sens.*, vol. 58, no. 5, pp. 561–567, May 1992.

[8] W. Carper, T. Lillesand, and R. Kiefer, "The use of intensity-hue-saturation transformations for merging SPOT panchromatic and multispectral image data," *Photogramm. Eng. Remote Sens.*, vol. 56, no. 4, pp. 459–467, 1990.

[9] T.-M. Tu, P. S. Huang, C.-L. Hung, and C.-P. Chang, "A fast intensity-hue-saturation fusion technique with spectral adjustment for IKONOS imagery," *IEEE Geosci. Remote Sens. Lett.*, vol. 1, no. 4, pp. 309–312, Oct. 2004.

[10] M. Gonzáles Audícana, X. Otazu, O. Fors, and J. A. Alvarez-Mozos, "A low computational-cost method to fuse IKONOS images using the spectral response function of its sensors," *IEEE Trans. Geosci. Remote Sens.*, vol. 44, no. 6, pp. 1683–1691, Jun. 2006.

[11] Y. Zhang, "Understanding image fusion," *Photogramm. Eng. Remote Sens.*, vol. 70, no. 6, pp. 657–661, Jun. 2004.

[12] C. A. Laben and B. V. Brower, "Process for enhancing the spatial resolution of multispectral imagery using Pan-sharpening," U.S. Patent 6 011 875, Jan. 4, 2000. Tech. Rep., Eastman Kodak Company.

[13] J. Núñez, X. Otazu, O. Fors, A. Prades, V. Palà, and R. Arbiol, "Multiresolution-based image fusion with additive wavelet decomposition," *IEEE Trans. Geosci. Remote Sens.*, vol. 37, no. 3, pp. 1204–1211, May 1999.

[14] T. Ranchin and L. Wald, "Fusion of high spatial and spectral resolution images: The ARSIS concept and its implementation," *Photogramm. Eng. Remote Sens.*, vol. 66, no. 1, pp. 49–61, Jan. 2000.

[15] B. Aiazzi, L. Alparone, S. Baronti, and A. Garzelli, "Context-driven fusion of high spatial and spectral resolution data based on oversampled multiresolution analysis," *IEEE Trans. Geosci. Remote Sens.*, vol. 40, no. 10, pp. 2300–2312, Oct. 2002.
[16] T. Ranchin, B. Aiazzi, L. Alparone, S. Baronti, and L. Wald, "Image fusion—The ARSIS concept and some successful implementation schemes," *ISPRS J. Photogramm. Remote Sens.*, vol. 58, no. 1/2, pp. 4–18, Jun. 2003.
[17] B. Aiazzi, L. Alparone, S. Baronti, A. Garzelli, and M. Selva, "MTF-tailored multiscale fusion of high-resolution MS and Pan imagery," *Photogramm. Eng. Remote Sens.*, vol. 72, no. 5, pp. 591–596, May 2006.
[18] M. Gonzáles Audícana, J. L. Saleta, R. García Catalán, and R. Garcia, "Fusion of multispectral and panchromatic images using improved IHS and PCA mergers based on wavelet decomposition," *IEEE Trans. Geosci. Remote Sens.*, vol. 42, no. 6, pp. 1291–1299, Jun. 2004.
[19] T.-M. Tu, S.-C. Su, H.-C. Shyu, and P. S. Huang, "A new look at IHS-like image fusion methods," *Inf. Fusion*, vol. 2, no. 3, pp. 177–186, Sep. 2001.
[20] L. Alparone, S. Baronti, A. Garzelli, and F. Nencini, "Landsat ETM+ and SAR image fusion based on generalized intensity modulation," *IEEE Trans Geosci. Remote Sens.*, vol. 42, no. 12, pp. 2832–2839, Dec. 2004.
[21] X. Otazu, M. Gonzáles Audícana, O. Fors, and J. Núñez, "Introduction of sensor spectral response into image fusion methods. Application to wavelet-based methods," *IEEE Trans. Geosci. Remote Sens.*, vol. 43, no. 10, pp. 2376–2385, Oct. 2005.
[22] S. M. Ross, *Introduction to Probability and Statistics for Engineers and Scientists*. Burlington, MA: Elsevier Academic, 2004.
[23] L. Wald, T. Ranchin, and M. Mangolini, "Fusion of satellite images of different spatial resolutions: Assessing the quality of resulting images," *Photogramm. Eng. Remote Sens.*, vol. 63, no. 6, pp. 691–699, 1997.
[24] L. Alparone, S. Baronti, A. Garzelli, and F. Nencini, "A global quality measurement of Pan-sharpened multispectral imagery," *IEEE Geosci. Remote Sens. Lett.*, vol. 1, no. 4, pp. 313–317, Oct. 2004.
[25] N. T. Lloyd and D. Bau, *Numerical Linear Algebra*, 3rd ed. Philadelphia, PA: Soc. Ind. Appl. Math., 1997.

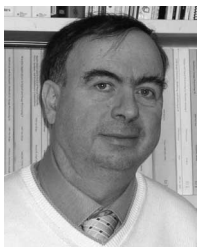

Bruno Aiazzi was born in Florence, Italy, in 1961. He received the Laurea degree in electronic engineering from the University of Florence, Florence, in 1991.

He was with the Italian Space Agency (ASI), working on SAR image analysis and classification, and with the European Space Agency (ESA), Centre National d'Etudes Spatiales (CNES), and the ASI, working on several international research projects on remote sensing research topics such as image quality definition and measurement, advanced methods for lossless and near-lossless data compression, and data fusion algorithms for environmental applications. After a period invested as a Research Assistant, since 2001, he has been a Researcher with the Institute of Applied Physics "Nello Carrara" CNR Area di Ricerca di Firenze (IFAC-CNR), Florence. He is the coauthor of about 30 papers published in international peer-reviewed journals.

Mr. Aiazzi received a Fellowship on Digital Image Processing and Compression, supported by the Italian National Research Council (CNR), in 1992 and the IEEE Geoscience and Remote Sensing Society Certificate of Appreciation as the winner of the 2006 Data Fusion Contest, *Fusion on Multispectral and Panchromatic Images*, from the IEEE Geoscience and Remote Sensing Society's Data Fusion Technical Committee.

Stefano Baronti (M'98) was born in Florence, Italy, in 1954. He received the Laurea degree in electronic engineering from the University of Firenze, Florence, in 1980.

He was with the Italian Highway Company. He joined the National Research Council of Italy in 1985, as a Researcher of the Institute of Applied Physics "Nello Carrara" CNR Area di Ricerca di Firenze (formerly, IROE-CNR), Florence, where he is currently a Senior Researcher. After an initial period spent on computer vision applications in the framework of European Union (ESPRIT) and Italian projects, he moved toward remote sensing by participating in and as the Head of several projects funded by the Italian, French, and European Space Agencies. His research interests include computer vision applications, image compression, processing of optical and microwave remote sensing SAR images, and fusion and quality assessment of remote sensing data. He is the coauthor of nearly 50 papers published in international peer-reviewed journals.

Mr. Baronti is a member of the IEEE Geoscience and Remote Sensing Society (GRSS) and the IEEE Signal Processing Society and participates in the GRSS Technical Committees on Data Fusion and on Data Archiving and Distribution. He is the recipient of the IEEE GRSS 2005 Letter Prize Paper Award and the IEEE Geoscience and Remote Sensing Society Certificate of Appreciation as the winner of the 2006 Data Fusion Contest, Fusion on Multispectral and Panchromatic Images, from the IEEE Geoscience and Remote Sensing Society's Data Fusion Technical Committee.

Massimo Selva was born in Florence, Italy in 1974. He received the Laurea degree (*summa cum laude*) in electronic engineering from the University of Florence, Florence, in 2001.

He is with the Institute of Applied Physics "Nello Carrara" CNR Area di Ricerca di Firenze (IFAC-CNR), Florence, working on remote sensing projects funded by the Italian and European Space Agencies and on activities for cultural heritage conservation as well. His main scientific interests include multiresolution image analysis, data fusion, and image quality assessment. He is an expert of C++, MATLAB, ENVI-IDL, and algorithm implementation aspects. He is a supporter of the Google search engine paradigm for verifying research ideas, solving information technology problems, and collecting data. He also likes investigating whether Jungian Psychoanalysis could be useful in improving people's research ability.